



HHS Public Access

Author manuscript

Mol Pharm. Author manuscript; available in PMC 2024 November 29.

Published in final edited form as:

Mol Pharm. 2023 September 04; 20(9): 4629–4639. doi:10.1021/acs.molpharmaceut.3c00360.

Evaluation of [⁸⁹Zr]Zr-DFO-2Rs15d Nanobody for Imaging of HER2-Positive Breast Cancer

Maxwell Ducharme,

Department of Radiology, University of Alabama at Birmingham, Birmingham, Alabama 35233, United States;

Lucinda Hall,

Department of Radiology, University of Alabama at Birmingham, Birmingham, Alabama 35233, United States;

Whitney Eckenroad,

Department of Radiology, University of Alabama at Birmingham, Birmingham, Alabama 35233, United States

Shelbie J. Cingoranelli,

Department of Radiology, University of Alabama at Birmingham, Birmingham, Alabama 35233, United States; Department of Chemistry, University of Alabama at Birmingham, Birmingham, Alabama 35233, United States

Hailey A. Houson,

Department of Radiology, University of Alabama at Birmingham, Birmingham, Alabama 35233, United States

Luke Jaskowski,

Department of Radiology, University of Alabama at Birmingham, Birmingham, Alabama 35233, United States; Department of Chemistry, University of Alabama at Birmingham, Birmingham, Alabama 35233, United States

Chanelle Hunter,

Department of Radiology, University of Alabama at Birmingham, Birmingham, Alabama 35233, United States

Benjamin M. Larimer,

Department of Radiology, University of Alabama at Birmingham, Birmingham, Alabama 35233, United States;

Suzanne E. Lapi

Department of Radiology, University of Alabama at Birmingham, Birmingham, Alabama 35233, United States; Department of Chemistry, University of Alabama at Birmingham, Birmingham, Alabama 35233, United States;

Corresponding Author: Suzanne E. Lapi – Department of Radiology, University of Alabama at Birmingham, Birmingham, Alabama 35233, United States; Department of Chemistry, University of Alabama at Birmingham, Birmingham, Alabama 35233, United States; lapi@uab.edu.

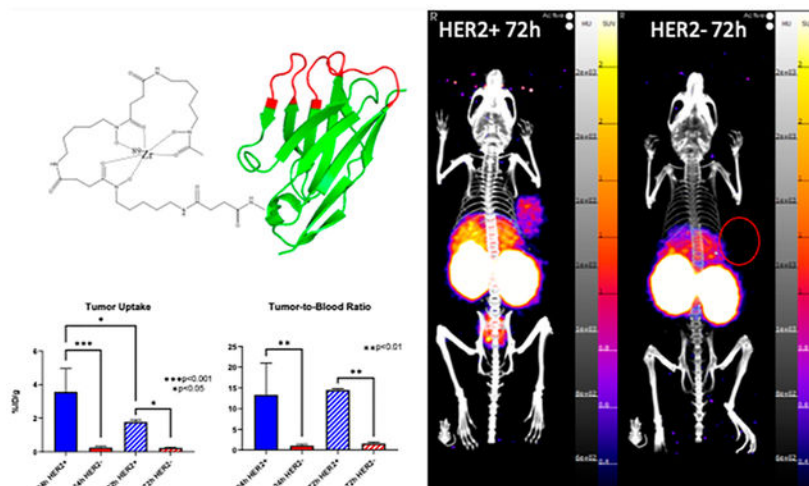
Complete contact information is available at: <https://pubs.acs.org/10.1021/acs.molpharmaceut.3c00360>

The authors declare no competing financial interest.

Abstract

One of the most aggressive forms of breast cancer involves the overexpression of human epidermal growth factor receptor 2 (HER2). HER2 is overexpressed in ~25% of all breast cancers and is associated with increased proliferation, increased rates of metastasis, and poor prognosis. Treatment for HER2-positive breast cancer has vastly improved since the development of the monoclonal antibody trastuzumab (Herceptin) as well as other biological constructs. However, patients still commonly develop resistance, illustrating the need for newer therapies. Nanobodies have become an important focus for potential development as HER2-targeting imaging agents and therapeutics. Nanobodies have many favorable characteristics, including high stability in heat and nonphysiological pH, while maintaining their low-nanomolar affinity for their designed targets. Specifically, the 2Rs15d nanobody has been developed for targeting HER2 and has been evaluated as a diagnostic imaging agent for single-photon emission computed tomography (SPECT) and positron emission tomography (PET). While a construct of 2Rs15d with the positron emitter ^{68}Ga is currently in phase I clinical trials, the only PET images acquired in preclinical or clinical research have been within 3 h postinjection. We evaluated our in-house produced 2Rs15d nanobody, conjugated with the chelator deferoxamine (DFO), and radiolabeled with ^{89}Zr for PET imaging up to 72 h postinjection. ^{89}Zr -DFO-2Rs15d demonstrated high stability in both phosphate-buffered saline (PBS) and human serum. Cell binding studies showed high binding and specificity for HER2, as well as prominent internalization. Our in vivo PET imaging confirmed high-quality visualization of HER2-positive tumors up to 72 h postinjection, whereas HER2-negative tumors were not visualized. Subsequent biodistribution studies quantitatively supported the significant HER2-positive tumor uptake compared to the negative control. Our studies fill an important gap in understanding the imaging and binding properties of the 2Rs15d nanobody at extended time points. As many therapeutic radioisotopes have single or multiday half-lives, this information will directly benefit the potential of the radiotherapy development of 2Rs15d for HER2-positive breast cancer patients.

Graphical Abstract



Keywords

PET; HER2; breast cancer; nanobody; imaging

INTRODUCTION

Breast cancer is diagnosed in 12% of women during their lifetime, making it the second most common cancer in women.^{1,2} One of the most aggressive forms of breast cancer involves the overexpression of the human epidermal growth factor receptor 2 (HER2). HER2 is a membrane tyrosine kinase that is a part of the HER family, which also includes HER1, HER3, and HER4 that are all involved in the regulation of normal breast growth and development.³ However, 15–25% of all breast cancer diagnoses have an overexpression of HER2, which leads to a poor prognosis and lower 5 year and overall survival rates.^{4–6} HER2 does not have any known natural binding ligands, but it is the preferred dimerization partner for the rest of the HER family.^{7,8} Moreover, HER2 has the strongest catalytic kinase activity, and HER2-containing heterodimers have the strongest signaling activity of any of the HER dimers.^{4,9} These signaling pathways include the mitogen-activated protein kinase (MAPK) and the phosphoinositide 3 kinase (PI3K) pathways, leading to downstream effects of cell proliferation, growth, and antiapoptosis.^{4,8,10} Treatments for HER2-positive breast cancer have evolved over the years, starting with the development of the monoclonal antibody trastuzumab (Herceptin) as the first-line treatment. Other antibodies, including pertuzumab (Perjeta) and the trastuzumab antibody-drug conjugate T-DM1 (Kadcyla), are also approved for the treatment of HER2-positive breast cancer. However, resistance can develop over time to both trastuzumab and pertuzumab.^{11–13} While the loss of HER2 is a common mechanism of resistance to these therapeutic agents, other methods of resistance, i.e., failure to trigger antibody-dependent cellular toxicity (ADCC) or increased drug-efflux pump activity show the need for continued development of other therapeutics which can overcome these HER2 alterations.¹⁴

The discovery of heavy-chain-only antibodies (HCAbs) and their single variable domains has led to the development of nanobodies as potential diagnostic and therapeutic biomolecules.^{15,16} Nanobodies are considered the smallest naturally derived antigen-binding fragments (~15 kDa) while still possessing affinities for their receptors in the low nanomolar range.¹⁵ Nanobodies have specific characteristics that differentiate them from monoclonal antibodies (mAbs). Nanobodies are a 10th of the size of mAb (~15 vs ~150 kDa), which leads to higher tissue penetration and a more rapid diffusion throughout the body. Moreover, they show low immunogenicity as well as resistance to harsh conditions, i.e., low and high pH and increased temperature.¹⁷ These favorable characteristics have led to the development of nanobodies as positron emission tomography (PET) imaging agents. Other antibody fragments have been evaluated for HER2 imaging, including affibodies. While affibodies have a smaller size (6–7 kDa), the main advantages of nanobodies over affibodies include greater stability for longer imaging times, higher affinity, and decreased likelihood of immune interaction due to the bacterial origin of affibodies.¹⁸

One nanobody that has been investigated for PET imaging is 2Rs15d. The 2Rs15d nanobody was developed from the inoculation of a dromedary with HER2-Fc recombinant protein to screen the HCABs for high-affinity HER2-binding nanobodies.¹⁹ Out of a screen of 38 nanobodies, 2Rs15d was described as having a K_d of 3.9 nM and showed no binding competition against trastuzumab or pertuzumab that bind to domains IV and II of the HER2 extracellular domain (ECD), respectively. This is an important property of a potential HER2 PET imaging agent since it can be used to monitor trastuzumab and/or pertuzumab therapy without competing for the same binding site.¹⁹ 2Rs15d has been shown to bind to the domain I of the HER2 ECD, confirming that 2Rs15d binds to a different epitope.²⁰ The 2Rs15d nanobody has since been evaluated as a PET imaging agent using both ⁶⁸Ga and ¹⁸F, resulting in high-quality images as quickly as 1 h postinjection in HER2-positive tumor xenograft mouse models.^{21,22} 2Rs15d has also been investigated as a therapeutic targeting agent using alpha emitters, including ²²⁵Ac and ²¹³Bi.^{23,24} With the emerging use of alpha emitters, with most half-lives between 10 h and 20 days, evaluating 2Rs15d for longer imaging time points may give insight into its ability to target HER2 for multiple days and thus the full capabilities for using alpha emitters combined with 2Rs15d for therapy. While 2Rs15d biodistribution at longer time points has been completed with the single-photon emission computed tomography (SPECT) imaging radioisotope ¹³¹I, to the best of our knowledge, no PET images have been acquired past 4 h postinjection. PET imaging has higher sensitivity and easier quantification compared to SPECT and could better evaluate the location of the nanobody in vivo.²⁵ This would be an important consideration for potential alpha emitter dosimetry and therapeutic potential, as this would allow for the acquisition of multiple PET images over time from a single injection of the radiolabeled nanobody.

The goal of this study was to evaluate the 2Rs15d nanobody for PET imaging using ⁸⁹Zr. Using ⁸⁹Zr, we were able to gain a greater understanding of the 2Rs15d nanobody's distribution multiple days after injection, which may aid in an understanding of the feasibility of 2Rs15d for use with longer-lived alpha emitters in the future.

EXPERIMENTAL SECTION

Chemicals and Reagents.

All chemicals were purchased from Thermo Fisher Scientific (Waltham, MA, USA) unless otherwise stated. Hydrochloric acid (HCl), sodium hydroxide (NaOH), and sodium phosphate were purchased from Millipore Sigma (Burlington, MA, USA). Deferoxamine-*p*-benzyl-isothiocyanate (DFO-Bz-NCS) was purchased from Macrocyclics (Plano, TX, USA). The UAB Cyclotron Facility prepared ⁸⁹Zr-oxalate according to previously published procedures.²⁶

Cell Culture.

MDA-MB-468 (HER2-) and BT474 (HER2+) cells were purchased from the American Type Culture Collection (Manassas, VA, USA). Both cell lines were grown in Gibco's high glucose Dulbecco's modified Eagle's medium (DMEM) supplemented with 10% fetal bovine serum (FBS) and 80 μ M gentamicin. The BT474 cell line media also had the addition of 1.8 mM of insulin. All cells were maintained and grown in humidified incubators at 37

°C with a 5% CO₂ atmosphere. DMEM media, FBS, and gentamicin were purchased from Thermo Fisher, and the insulin was purchased from Millipore Sigma.

Production and Purification of the 2Rs15d Nanobody.

The coding sequence of the 2Rs15d nanobody was modified to contain C-terminal FLAG and 6× His sequences for detection, and NTA-Ni²⁺ purification was codon optimized for *Escherichia coli* expression and chemically synthesized (Integrated DNA Technologies, Coralville, Iowa, USA).²⁰ The synthesized sequence was cloned into the pET22b(+) expression vector using NcoI and XhoI restriction sites and transformed into BL21 in one shot (DE3) Chemically Competent *E. coli* (Invitrogen). Recombinant nanobody was isolated via periplasmic extraction and purified by immobilized metal affinity chromatography using a GE AKTA FPLC instrument with a HisTrap HP 5 mL NTA-Ni²⁺ resin column (Cytiva Life Sciences). Additional purification of the nanobody was achieved by size exclusion chromatography. Fractions containing nanobodies were identified via the UV peaks on the FPLC and verified via running SDS-PAGE gels. The nanobody-containing fractions were then buffer-exchanged using a 0.5 mL 3 K spin column (Millipore) and diluted in phosphate buffer saline (PBS).

2Rs15d Conjugation.

The 2Rs15d nanobody was buffer-exchanged in 1× PBS (pH ~ 7) using a 0.5 mL 7 K MWCO Zeba Spin Desalting Column before conjugation. DFO-Bz-NCS was dissolved in dimethyl sulfoxide (DMSO) at a concentration of 2 µg/µL (2.6 mM). A five times molar excess of DFO-Bz-NCS was added to the 2Rs15d nanobody with 30 µL of 0.1 M sodium carbonate (pH 9) for a final pH of ~8.5. The solution was maintained at room temperature overnight while being shaken at 1200 rpm. The solution was purified using a fresh 0.5 mL 7 K MWCO Zeba Spin Desalting Column and buffer-exchanged into 1 M HEPES (pH 7) to remove any excess DFO-Bz-NCS.

Radiolabeling of DFO-2Rs15d with ⁸⁹Zr-Oxalate.

⁸⁹Zr-oxalate was neutralized using 1 M HEPES and 5 M NaOH to a pH of 7 before labeling. ~3 µL (10 µg) of conjugated and purified DFO-2Rs15d, 10 µL (37 MBq) of neutralized ⁸⁹Zr-oxalate, and 15–20 µL of 1 M HEPES were combined and incubated at 37 °C while shaking at 1200 rpm for 1 h. Instant thin-layer chromatography (iTLC) using silica-embedded iTLC plates was used to determine radiolabeling efficiency and analyzed on an Eckert & Ziegler AR-2000 radio-TLC scanner. iTLC plates were developed in a 50 mM DTPA solution. No purification was required for radiolabeling >95% efficiency.

Stability of [⁸⁹Zr]Zr-DFO-2Rs15d.

Ten µg of [⁸⁹Zr]Zr-DFO-2Rs15d was added to 100 µL of PBS or human serum (human origin; Fisher Scientific; lot 207624) and incubated at 37 °C while shaking for 800 rpm. For iTLC analysis, 1 µL aliquots were taken at 1, 4, 24, 72, 120, and 168 h. Intact [⁸⁹Zr]Zr-DFO-2Rs15d was determined by drawing regions of interest (ROIs) of radioactivity and comparing them with the initial peak of unbound ⁸⁹Zr ($R_f \sim 0.26$) and the [⁸⁹Zr]Zr-

DFO-2Rs15d peak ($R_f = 0.0$). Studies were repeated twice with 3 samples each for a total of $n = 6$ per medium.

Cell Binding, Specificity, and Internalization Studies.

For cell binding experiments, 2.5×10^5 of MDA-MB-468 and BT474 cells were seeded in 24-well plates 48 h before the experiments. Cells were washed with room temperature PBS once before nanobody incubation. Cells were incubated at room temperature for 1 h with 0.5 mL of 10 nM [^{89}Zr]Zr-DFO-2Rs15d solution only, [^{89}Zr]Zr-DFO-2Rs15d with 500 nM of unlabeled 2Rs15d, or [^{89}Zr]Zr-DFO-2Rs15d with 500 nM of trastuzumab, all in PBS, to determine cell specificity to HER2 and binding competition with trastuzumab (all groups $n = 8$). After incubation, the initial PBS was removed, and cells were washed in triplicate with ice-cold PBS. Cells were removed from the plate with 250 μL of 1 M NaOH, and all contents within each individual well were collected into microcentrifuge tubes. A final wash of 250 μL of PBS was used to remove all contents and was pipetted into the same tube. Activity per well was evaluated on a HIDEX AMG gamma counter (HIDEX Oy, Turku, Finland). Values were normalized to total protein concentration per well determined by a BCA assay (Thermo Fisher) to give final values in percent activity per mg of protein (% activity/mg).

A similar procedure was followed for cell internalization studies, with a few modifications. Five $\times 10^5$ BT474 cells were plated in 12-well plates ($n = 6$) 48 h prior to the experiment. Cells were incubated with 0.5 mL of 10 nM of [^{89}Zr]Zr-DFO-2Rs15d in complete media for either 1, 2, 4, 24, or 72 h at 37 °C. After incubation, media was removed, and cells were washed in triplicate with ice-cold PBS. To isolate and recover the surface-bound [^{89}Zr]Zr-DFO-2Rs15d, cells were incubated once with 250 μL of an acid wash (0.1 M sodium citrate buffer pH ~ 2) for 5 min at room temperature. The acid wash was collected separately, the cells were removed, and activity was determined as described previously.

Biodistribution and Imaging of [^{89}Zr]Zr-DFO-2Rs15d.

The animal study protocol (protocol IACUC-21530) was approved by the Institutional Animal Care and Use Committee of The University of Alabama at Birmingham in February 2019. Female athymic nude mice at 5 weeks of age were purchased from Charles River Laboratories (Wilmington, MA, USA). After 1 week of acclimation, homemade estrogen pellets were implanted into the right shoulder of mice who would be implanted with BT474 cells to aid in the frequency and growth of the BT474 xenografts. The pellet was made by combining 0.72 mg of β -estradiol with 19.28 mg of cholesterol in a pestle and mortar until it was fine and homogeneous. Using a hand-sized tabletop pellet press, 20 mg of total powder was pressed using a hammer to form pellets. One week after pellet implantation, mice were injected with 10^7 cells in a 1:1 ratio of normal Matrigel and PBS ($\sim 150 \mu\text{L}$) of either MDA-MB-468 (HER2 $-$) or BT474 (HER2 $+$) in their left shoulder. Tumors were allowed to grow until palpable (approximately $5 \times 5 \times 5$ mm) about 4 to 6 weeks after injection. Mice were injected with 8.5 μg of [^{89}Zr]Zr-DFO-2Rs15d (0.5 nmol: ~ 2.6 MBq) in 100 μL of a mixture of sterile water and sterile saline to achieve a final osmolality of 300 mOsm. Mice were anesthetized with 2.5% isoflurane in oxygen for injections and PET/CT imaging acquisition. In between injections and imaging, mice were allowed to roam freely in their cages. Mice

were imaged 24 h postinjection on a Sofie GNEXT PET/CT with an acquisition time of 20 min followed by a 5 min CT at 80 kVp, at 48 h (25 min PET acquisition, 5 min CT) and 72 h (30 min PET acquisition, 5 min CT). Groups of HER2-positive and HER2-negative tumor-bearing mice were immediately euthanized after the 24 and 72 h imaging time points for biodistribution. After euthanasia, organs were dissected and weighed, and radioactivity was measured on a HIDEX AMG automated gamma counter. The uptake of radioactivity was calculated as the percent injected dose per gram of tissue (% ID/g).

PET images were reconstructed with a 3D ordered subset expectation maximization (OSEM) algorithm (24 subsets and 3 iterations), with random, attenuation, and decay correction, and CT images were reconstructed with the modified Feldkamp algorithm and analyzed using VivoQuant (Invivo) software. After images were reconstructed, standard uptake values (SUVs) were determined by hand-drawing regions of interest (ROIs) from both the HER2-positive and HER2-negative tumors and an adjacent muscle within the same mouse using CT anatomical guidelines. Radioactivity in each ROI was calculated as the SUV (eq 1).

$$SUV = \frac{\text{concentration of radioactivity in tumor} \left(\frac{\text{MBq}}{\text{mL}} \right)}{\text{injected radioactivity (MBq) / mouse weight (g)}} \quad (1)$$

Statistical Analysis.

Quantitative analysis was expressed as mean \pm SD. Comparisons were made using Prism 8 software running an ordinary one-way ANOVA with multiple comparisons, unless otherwise stated. *P* values of less than 0.05 were considered significant.

RESULTS

2Rs15d Production and Purification.

2Rs15d was expressed and purified through SEC and isolated in fraction 6 of the FPLC method (Figure 1A). A sample from fraction 6 was run on SDS-PAGE and had a confirmed mass of ~17 kDa (Figure 1B). After confirmation of 2Rs15d and qualitative purity through SDS-PAGE, the fraction was concentrated, further purified through the 3 kDa spin column, and buffer-exchanged to yield the starting material in PBS.

Molar Activity and Stability of [⁸⁹Zr]Zr-DFO-2Rs15d.

DFO was conjugated to 2Rs15d and resulted in an average protein recovery of 86.5 \pm 12.8% after purification. Radiolabeling of DFO-2Rs15d with ⁸⁹Zr resulted in radiolabeling percentages >95% confirmed by iTLC. Radiolabeling purity was determined before all in vitro and in vivo experiments. The molar activity of [⁸⁹Zr]Zr-DFO-2Rs15d ranged between 2.5 and 6.20 MBq/nmol.

[⁸⁹Zr]Zr-DFO-2Rs15d showed high stability in human serum and PBS for up to 7 days (Figure 2). While there was a modest decrease of intact [⁸⁹Zr]Zr-DFO-2Rs15d over time,

[⁸⁹Zr]Zr-DFO-2Rs15d was 77.0 ± 5.2 and $80.3 \pm 11.8\%$ intact after 7 days in human serum and PBS, respectively.

In Vitro Cell Binding and Cell Internalization Studies of [⁸⁹Zr]Zr-DFO-2Rs15d.

[⁸⁹Zr]Zr-DFO-2Rs15d with a purity of >95% was used for cell studies. Cell binding and blocking studies were performed to investigate the specific binding to HER2 (Figure 3A). There was significantly higher uptake (percent radioactivity per mg of total protein) in HER2-positive BT474 cells compared to HER2-negative MDA-MB-468 cells (54.7 ± 2.6 versus 6.1 ± 0.6 ; $p < 0.0001$), indicating binding to HER2. Specificity for HER2 was further shown through cell-blocking studies with unlabeled DFO-2Rs15d. There was a significant decrease in binding of [⁸⁹Zr]Zr-DFO-2Rs15d when blocking with unlabeled DFO-2Rs15d (54.7 ± 2.6 versus 13.5 ± 3.4 ; $p < 0.0001$). Blocking with trastuzumab did show a significant difference in the amount of binding of [⁸⁹Zr]Zr-DFO-2Rs15d (54.7 ± 2.6 versus 50.1 ± 3.1 ; $p < 0.01$). While there was a significant difference in the amount of binding of [⁸⁹Zr]Zr-DFO-2Rs15d, it is likely that the slight decrease in binding with the trastuzumab blocking group is most likely due to the occupation and internalization of HER2 initiated by trastuzumab binding. This is supported by the drastic difference in [⁸⁹Zr]Zr-DFO-2Rs15d binding between the trastuzumab (50.1 ± 3.1) and unlabeled DFO-2Rs15d (6.1 ± 0.6) blocking groups.

The BT474 cells were used to determine the internalization of [⁸⁹Zr]Zr-DFO-2Rs15d over time (Figure 3B). As early as 1 h after incubation, $48.5 \pm 0.8\%$ of the activity associated with the cells was internalized, with a steady increase in the amount of cell-associated [⁸⁹Zr]Zr-DFO-2Rs15d internalized over time to $95.2 \pm 0.2\%$ after 72 h.

PET Imaging and Biodistribution.

[⁸⁹Zr]Zr-DFO-2Rs15d preparations for PET imaging and biodistribution studies were confirmed to have a purity of >95% before injection. Athymic nude mice bearing tumor xenografts were injected with [⁸⁹Zr]Zr-DFO-2Rs15d and imaged at 24, 48, and 72 h postinjection. HER2-positive tumors could be visualized by PET (Figure 4) after image reconstruction, while clear identification of HER2-negative tumors in the same signal window was not possible on PET images alone (Figure 5).

ROIs of tumors yielded mean standard uptake value (SUV_{mean}) values (Figure 6) for HER2-positive tumors, which were significantly higher than the HER2-negative tumors at all time points (24 h: 0.7 ± 0.1 versus 0.1 ± 0.0 /48 h: 0.6 ± 0.1 versus 0.1 ± 0.0 /72 h: 0.5 ± 0.0 versus 0.1 ± 0.0 ; $p < 0.0001$ for all time points).

The biodistribution data support the findings from the PET imaging data of both HER2-positive and HER2-negative tumor-bearing mice at 24 and 72 h (Figure 7A,B). Kidneys showed the highest amount of radioactivity at both time points (>100% ID/g), which is expected due to the known excretion pathway of [⁸⁹Zr]Zr-DFO-2Rs15d through the kidneys. The mice bearing the MDA-MB-468 (HER2-) tumors had higher kidney uptake than the BT474 (HER2+) tumors at both time points, including a significant difference at 24 h (179.4 ± 47.8 versus 100.2 ± 23.7 ; $p < 0.05$). There was modest uptake in the liver (~3% ID/g) and spleen (~2% ID/g) in all groups. The femur also showed some uptake (0.3–1.3% ID/g). At

both time points, femur uptake was significantly higher in our HER2+ tumor-bearing mice versus HER2- tumor-bearing mice (24 h: 1.3 ± 0.3 versus 0.3 ± 0.1 ; $p < 0.01$ /72 h: 0.7 ± 0.1 versus 0.4 ± 0.0 ; $p < 0.001$). The rest of the vital organs had low uptake at $<0.5\%$ ID/g.

There was a significant difference in tumor uptake with HER2-positive BT474 tumors compared to that with HER2-negative MDA-MB-468 tumors (Figure 7C). At 24 h, HER2-positive tumors had an uptake of $3.6 \pm 1.4\%$ ID/g, which was significantly higher than the HER2-negative tumors ($0.3 \pm 0.1\%$ ID/g; $p < 0.001$). There was a similar significance difference between the HER2-positive and HER2-negative tumors at 72 h ($1.8 \pm 0.1\%$ ID/g versus $0.2 \pm 0.0\%$ ID/g; $p < 0.05$). HER2-positive tumor binding was significantly higher at 24 h versus 72 h ($3.6 \pm 1.4\%$ ID/g versus $1.8 \pm 0.1\%$ ID/g; $p < 0.05$). There was also a significant difference in tumor-to-blood ratios between the HER2-positive and HER2-negative tumor mice at both 24 and 72 h (24 h: 13.3 ± 7.7 versus 1.0 ± 0.4 ; $p < 0.01$ /72 h: 14.5 ± 0.3 versus 1.6 ± 0.3 ; $p < 0.01$; Figure 7D). Tumor-to-muscle ratios were also significantly higher at 24 and 72 h for HER2-positive tumor-bearing mice compared to HER2-negative tumor-bearing mice (24 h: 39.9 ± 29.0 versus 2.5 ± 1.0 ; $p < 0.05$ /72 h: 18.8 ± 2.1 versus 2.4 ± 1.0 ; $p < 0.0001$).

DISCUSSION

Identification of HER2-positive breast cancer with PET imaging with radiolabeled trastuzumab and pertuzumab has been an important area of research to help understand which patients would benefit from HER2-targeted therapy.^{27–35} Patients whose lesions show high uptake of the antibodies are likely to be positive responders to antibody-based therapies. The ZEPHIR trial showed that out of 39 HER2-positive patients, 28 patients (71.8%) showed objective response, whereas 14 out of 16 HER2-negative patients (87.5%) had stable or progressive disease with trastuzumab emtansine (T-DM1) treatment.²⁸ However, HER2-positive breast cancer has been shown to become resistant to antibody-based therapy through a variety of mechanisms.^{11–14} Development of new specific-targeting therapeutic agents that utilize other methods, including radiotherapy, is showing progress in several cancer types. Our studies evaluated the 2Rs15d nanobody for PET imaging of HER2-positive breast cancer with ⁸⁹Zr. ⁸⁹Zr has a half-life of 78.4 h with an average positron energy of 395.5 keV, which gives it favorable characteristics including good imaging resolution and a half-life which permits imaging several days postinjection.³⁶ While there have been preclinical studies with 2Rs15d at longer time points using ¹³¹I, the improved spatial resolution for PET imaging is an advantage worth exploring. These are the first preclinical PET images acquired for the 2Rs15d nanobody radiolabeled with the positron-emitter ⁸⁹Zr. As 2Rs15d is drawing interest for use in radiotherapy, it is important to evaluate the biodistribution of 2Rs15d at longer time points to understand the potential dosimetry of the radiolabeled 2Rs15d before exposure to therapeutic radioisotopes that give a high amount of ionizing radiation. This study allowed us to evaluate the biodistribution of 2Rs15d at longer time points and show that ⁸⁹Zr could be a suitable isotope for these imaging studies. PET image acquisition utilizing [⁸⁹Zr]Zr-DFO-2Rs15d will give insight into the extended time points, which will be beneficial to gain a better understanding of the long-term binding capabilities, tumor retention, and off-target effects of the radiotherapeutics.

Our in-house-prepared 2Rs15d was successfully conjugated to deferoxamine (DFO) and efficiently radiolabeled with ^{89}Zr showing the first DFO- ^{89}Zr labeling of the 2Rs15d nanobody. This also showed that bifunctional chelators possessing the R-Bn-NCS moiety can be conjugated to the 2Rs15d nanobody in a similar procedure as antibodies.³⁷ To show in vitro stability, serum and PBS stability studies were performed and showed that ~80% of the original nanobody remained intact after 7 days of incubation.

The in vitro binding properties of [^{89}Zr]Zr-DFO-2Rs15d showed significantly higher binding (% activity/mg of total protein) in the HER2-overexpressing BT474 cells compared to the triple-negative MDA-MB-468 cells (54.7 ± 2.6 versus 6.1 ± 0.6 ; $p < 0.0001$). Specificity for HER2 was indicated by blocking the binding of [^{89}Zr]Zr-DFO-2Rs15d using unlabeled DFO-2Rs15d (54.7 ± 2.6 versus 13.5 ± 3.4 ; $p < 0.0001$). Somewhat surprisingly, the addition of trastuzumab resulted in a modest decrease in 2Rs15d binding (54.7 ± 2.6 versus 50.1 ± 3.1 ; $p < 0.01$). It was first described by D'Huyvetter et al. that 2Rs15d binds to domain I of the extracellular domain, different from trastuzumab or pertuzumab.²⁰ Trastuzumab has been shown to bind to domain IV on the extracellular domain.^{11,38,39} It has also been shown that trastuzumab binding to HER2 can induce internalization.⁴⁰ A possible explanation for lower nanobody binding is that the addition of the higher molar value (500 nM) of trastuzumab occupied the HER2 receptor and led to the decrease of HER2 on the cell surface via internalization, thus leading to less HER2 availability for binding of [^{89}Zr]Zr-DFO-2Rs15d. While there was a significant difference in binding with the addition of trastuzumab, the amount of binding in the trastuzumab blocking group (50.1 ± 3.1) was significantly higher than the unlabeled 2Rs15d blocking group (13.5 ± 3.4 ; $p < 0.0001$), indicating that true epitope blocking was most likely not the factor that caused lower binding.

Our studies showed that [^{89}Zr]Zr-DFO-2Rs15d was internalized at $48.5 \pm 0.8\%$ after 1 h and $95.2 \pm 0.2\%$ after 72 h. Previous internalization studies with 2Rs15d derivatives showed only ~9% of nanobody was internalized after 1 h and ~29% after 24 h.²⁰ The current study's 24 h time point showed $83.5 \pm 0.4\%$ was internalized, which may be caused by modifications of our nanobody, including the 6 \times His-tag, sortase, and FLAG, which can alter the internalization or efflux of the nanobody from the cell. It is also possible that the amount of efflux differs with ^{89}Zr as compared to other radioisotopes such as ^{18}F , which has different chemical properties. It has been hypothesized that after internalization, ^{89}Zr will bind to intracellular components, decreasing the efflux out of the cell.⁴¹ The combination of high binding to HER2 and a high internalization rate shows that 2Rs15d has a high potential for continued therapeutic development.

In vivo evaluation of [^{89}Zr]Zr-DFO-2Rs15d was completed with PET image acquisition at 24, 48, and 72 h postinjection and biodistribution at 24 and 72 h. HER2-positive tumor uptake was significantly higher at 24 h than at 72 h (3.6 ± 1.4 versus $1.8 \pm 0.1\%$ ID/g; $p < 0.05$). Similar biodistribution studies showed similar values of 3.6 ± 0.3 and $2.9 \pm 0.6\%$ ID/g of ^{177}Lu -DTPA-2Rs15d and 5.1 ± 1.9 and $0.4 \pm 0.1\%$ ID/g of ^{131}I -2Rs15d at 24 and 72 h, respectively.^{20,42} It is important to note that the ^{177}Lu -DTPA-2Rs15d was evaluated in a cell model (SKOV3) different from our BT474 cell model. This, combined with a different chelator/isotope combination, may lead to a difference in values. The [^{89}Zr]Zr-DFO-2Rs15d

nanobody had the highest uptake in the kidneys (>100% ID/g) at all time points, which may be a dosimetry concern when developing radiotherapeutics. We expected that the kidneys would have the highest uptake since nanobodies are excreted through the kidneys. It has also been shown that the nanobody is retained in the proximal tubule of the kidney cortex.⁴³ Our nanobody was purified using a nickel column and still possesses a histidine tag used for association with the nickel column. Studies with the his-tagged version of 2Rs15d have also been completed by Xavier et al. using ⁶⁸Ga at a 1 h postinjection time point.²² The tumor uptake at 1 h was reported at $3.1 \pm 0.1\%$ ID/g, with a tumor-to-blood ratio of 9.5 ± 2.9 . In comparison, we have tumor uptakes of 3.6 ± 1.4 and 1.8 ± 0.1 with tumor-to-blood ratios of 13.3 ± 7.7 and 14.5 ± 0.3 at 24 and 72 h, respectively. This data supports the previous data with PET imaging of 2Rs15d but also lays the foundation for using the ⁸⁹Zr-labeled 2Rs15d for PET imaging for multiple days postinjection. Currently, in clinical trials, ⁶⁸Ga-2Rs15d is only imaged 1–2 h postinjection. We believe that imaging with ⁸⁹Zr may allow us to image a patient multiple times through one injection. Gaining this insight supports using 2Rs15d for potential radiotherapy. Future development of this nanobody will include the removal of the histidine tag, as it has been shown to decrease kidney retention.^{22,42,44} Other methods to decrease kidney retention include the injection of gelofusine, which works by reducing the amount of binding and uptake of radiopharmaceuticals that are excreted by the kidneys.⁴² Decreasing kidney retention would be a significant focus for developing 2Rs15d for potential use for radiotherapy. The remaining vital organs showed low uptake 72 h postinjection. The liver and spleen were the only organs that showed uptake $\sim 1\%$ ID/g, suggesting that off-target binding and uptake of the [⁸⁹Zr]Zr-DFO-2Rs15d were minimal. While the femur contained $\sim 1\%$ ID/g at the 24 and 72 h time points, this may be attributed to the unbound ⁸⁹Zr decoupled from the nanobody after being metabolized. There was significantly higher uptake in the femur in our HER2-positive tumor mice than in the HER2-negative tumor mice. An explanation for this result could be a difference in excretion between the HER2-positive tumor and HER2-negative tumor mice, as indicated by the difference in kidney uptake between the models. Once decoupled from the nanobody, or more specifically, the DFO chelator, free ⁸⁹Zr is known to localize in the bone in mice.⁴⁵ However, we were able to clearly visualize HER2-positive tumors at 24, 48, and 72 h postinjection, which is the first PET image acquired past 3 h using this nanobody to the best of our knowledge. While ⁶⁴Cu ($t_{1/2} = 12.7$ h) could have also been a suitable isotope for our studies, ⁸⁹Zr ($t_{1/2} = 78.4$ h) had greater advantages with its longer half-life. At our 72 h time point, only $\sim 2\%$ of the starting dose of ⁶⁴Cu would be left, whereas with ⁸⁹Zr, there is 53% remaining when considering physical decay. Using ⁸⁹Zr for both time points gave us a more direct comparison and provided sufficient radioactivity for our later time point.

Peptides have also been evaluated for HER2 PET imaging but do not favorably compare with respect to the binding capabilities of antibodies or nanobodies. The KCCYSL peptide motif is the most evaluated and resulted in a tumor uptake range of $0.34 \pm 0.03\%$ ID to $0.66 \pm 0.11\%$ ID/g at 2 h postinjection.^{46–48} Affibodies have also been evaluated in clinical trials but struggle with affinity, off-target binding, and expensive production.^{18,49} Antibodies will have a superior binding ability with low nanomolar affinity; however, we believe that [⁸⁹Zr]Zr-DFO-2Rs15d has strong characteristics for binding affinity, stability, and imaging potential.

2Rs15d has been evaluated preclinically using a variety of different therapeutic isotopes including the beta-emitter ^{177}Lu , and the alpha-emitters ^{213}Bi , ^{211}At , and ^{225}Ac .^{23,42,50,51} While it was shown that ^{177}Lu -DTPA-2Rs15d can target SKOV3 tumors as described earlier, there are some advantages of using alpha emitters over beta emitters for therapy. Alpha emitters can deliver a higher linear energy transfer than beta emitters and have a shorter distance at which they cause ionizing radiation.⁵² Pruszynski et al. evaluated ^{225}Ac -DOTA-2Rs15d up to 48 h postinjection and observed $1.3 \pm 0.2\%$ ID/g in HER2-positive tumors with relatively low kidney retention ($7.6 \pm 1.0\%$ ID/g).²⁴ Rodak et al. also reported ^{225}Ac -DOTA-2Rs15d uptake in SKOV3 (HER2-positive) tumors of 6.2 ± 1.0 and $4.2 \pm 0.7\%$ ID/g at 48 and 72 h, respectively.⁵³ Our biodistribution data illustrated [^{89}Zr]Zr-DFO-2Rs15d uptake in HER2-positive tumors up to 72 h postinjection ($1.8 \pm 0.1\%$ ID/g), as well as the highest tumor-to-blood ratio (14.5 ± 0.3), while studies at 24 h illustrated higher tumor uptake ($3.6 \pm 1.4\%$ ID/g). This work illustrates that continued evaluation and potential modifications to the 2Rs15d nanobody may be needed for longer time points to optimize use with ^{225}Ac ($t_{1/2} = 9.9$ d).

Our work demonstrates that the 2Rs15d nanobody can specifically target HER2-positive tumors up to 3 days after injection. 2Rs15d can potentially be used to identify HER2-positive lesions, to monitor treatment during current first-line antibody therapy, and has potential future use as a radiotherapeutic. The continued development of this nanobody will be to extend imaging time points past 72 h and to decrease the amount of kidney binding and retention to improve pharmacokinetics and thus decrease the amount of dose to the kidneys.

CONCLUSIONS

2Rs15d was successfully conjugated with DFO to support radiolabeling with ^{89}Zr . [^{89}Zr]Zr-DFO-2Rs15d showed specific binding to HER2 and high in vitro stability for up to 7 days in human serum. In vivo evaluation confirmed that specific targeting of HER2-positive tumors could be achieved up to 72 h postinjection, yielding the first PET targeting agent based on 2Rs15d to be evaluated past 4 h. [^{89}Zr]Zr-DFO-2Rs15d uptake was visualized up to 72 h postinjection in HER2-positive tumor-bearing mice, whereas HER2-negative tumors were not distinguished using PET. Overall, our work supports the continued development of the 2Rs15d nanobody for HER2 PET imaging as well as supports further investigation for radiotherapeutic use.

ACKNOWLEDGMENTS

We would like to thank the UAB Cyclotron Facility for the production and purification of ^{89}Zr .

Funding

This work was supported by the Department of Radiology at the University of Alabama at Birmingham. Imaging studies were supported by the UAB Small Animal Imaging Facility (supported by the O'Neal Comprehensive Cancer Center at UAB, P30CA013148).

REFERENCES

- (1). Waks AG; Winer EP Breast cancer treatment: a review. *Jama* 2019, 321, 288–300. [PubMed: 30667505]

- (2). Bray F; Ferlay J; Soerjomataram I; Siegel RL; Torre LA; Jemal A Global cancer statistics 2018: GLOBOCAN estimates of incidence and mortality worldwide for 36 cancers in 185 countries. *Ca-Cancer J. Clin* 2018, 68, 394–424. [PubMed: 30207593]
- (3). Yarden Y Biology of HER2 and its importance in breast cancer. *Oncology* 2001, 61, 1–13.
- (4). Gutierrez C; Schiff R HER2: biology, detection, and clinical implications. *Arch. Pathol. Lab. Med* 2011, 135, 55–62. [PubMed: 21204711]
- (5). Slamon DJ; Godolphin W; Jones LA; Holt JA; Wong SG; Keith DE; Levin WJ; Stuart SG; Udove J; Ullrich A; et al. Studies of the HER-2/neu proto-oncogene in human breast and ovarian cancer. *Science* 1989, 244, 707–712. [PubMed: 2470152]
- (6). Krishnamurti U; Silverman JF HER2 in breast cancer: a review and update. *Adv. Anat. Pathol* 2014, 21, 100–107. [PubMed: 24508693]
- (7). Graus-Porta D; Beerli RR; Daly JM; Hynes NE ErbB-2, the preferred heterodimerization partner of all ErbB receptors, is a mediator of lateral signaling. *EMBO J.* 1997, 16, 1647–1655. [PubMed: 9130710]
- (8). Marchiò C; Annaratone L; Marques A; Casorzo L; Berrino E; Sapino A Evolving concepts in HER2 evaluation in breast cancer: Heterogeneity, HER2-low carcinomas and beyond. *Semin. Cancer Biol* 2021, 72, 123–135. [PubMed: 32112814]
- (9). Moasser MM The oncogene HER2: its signaling and transforming functions and its role in human cancer pathogenesis. *Oncogene* 2007, 26, 6469–6487. [PubMed: 17471238]
- (10). Paplomata E; O'Regan R The PI3K/AKT/mTOR pathway in breast cancer: targets, trials and biomarkers. *Ther. Adv. Med. Oncol* 2014, 6, 154–166. [PubMed: 25057302]
- (11). Pohlmann PR; Mayer IA; Mernaugh R Resistance to trastuzumab in breast cancer. *Clin. Cancer Res* 2009, 15, 7479–7491. [PubMed: 20008848]
- (12). de Melo Gagliato D; Leonardo Fontes Jardim D; Marchesi MSP; Hortobagyi GN Mechanisms of resistance and sensitivity to anti-HER2 therapies in HER2+ breast cancer. *Oncotarget* 2016, 7, 64431–64446. [PubMed: 26824988]
- (13). Zhang Y; Wu S; Zhuang X; Weng G; Fan J; Yang X; Xu Y; Pan L; Hou T; Zhou Z; et al. Identification of an Activating Mutation in the Extracellular Domain of HER2 Conferring Resistance to Pertuzumab. *OncoTargets Ther.* 2019, 12, 11597–11608.
- (14). Schlam I; Tarantino P; Tolaney SM Overcoming Resistance to HER2-Directed Therapies in Breast Cancer. *Cancers* 2022, 14, 3996. [PubMed: 36010990]
- (15). Muyldermans S Applications of nanobodies. *Annu. Rev. Anim. Biosci* 2021, 9, 401–421. [PubMed: 33233943]
- (16). Yang EY; Shah K Nanobodies: next generation of cancer diagnostics and therapeutics. *Front. Oncol* 2020, 10, 1182. [PubMed: 32793488]
- (17). Steeland S; Vandembroucke RE; Libert C Nanobodies as therapeutics: big opportunities for small antibodies. *Drug discovery today* 2016, 21, 1076–1113. [PubMed: 27080147]
- (18). Altunay B; Morgenroth A; Beheshti M; Vogg A; Wong NC; Ting HH; Biersack H-J; Stickeler E; Mottaghy FM HER2-directed antibodies, affibodies and nanobodies as drug-delivery vehicles in breast cancer with a specific focus on radioimmunotherapy and radioimmunoinaging. *Eur. J. Nucl. Med. Mol. Imaging* 2021, 48, 1371–1389. [PubMed: 33179151]
- (19). Vaneycken I; Devoogdt N; Van Gassen N; Vincke C; Xavier C; Wernery U; Muyldermans S; Lahoutte T; Cavelliers V Preclinical screening of anti-HER2 nanobodies for molecular imaging of breast cancer. *FASEB J.* 2011, 25, 2433–2446. [PubMed: 21478264]
- (20). D'Huyvetter M; De Vos J; Xavier C; Pruszynski M; Sterckx YG; Massa S; Raes G; Cavelliers V; Zalutsky MR; Lahoutte T; et al. 131I-labeled Anti-HER2 Camelid sdAb as a Theranostic Tool in Cancer Treatment. *Clin. Cancer Res* 2017, 23, 6616–6628. [PubMed: 28751451]
- (21). Zhou Z; Vaidyanathan G; McDougald D; Kang CM; Balyasnikova I; Devoogdt N; Ta AN; McNaughton BR; Zalutsky MR Fluorine-18 labeling of the HER2-targeting single-domain antibody 2Rs15d using a residualizing label and preclinical evaluation. *Mol. Imaging Biol* 2017, 19, 867–877. [PubMed: 28409338]
- (22). Xavier C; Vaneycken I; D'huyvetter M; Heemskerk J; Keyaerts M; Vincke C; Devoogdt N; Muyldermans S; Lahoutte T; Cavelliers V Synthesis, preclinical validation, dosimetry, and

- toxicity of ^{68}Ga -NOTA-anti-HER2 Nanobodies for iPET imaging of HER2 receptor expression in cancer. *J. Nucl. Med* 2013, 54, 776–784. [PubMed: 23487015]
- (23). Dekempeneer Y; Caveliers V; Ooms M; Maertens D; Gysemans M; Lahoutte T; Xavier C; Lecocq Q; Maes K; Covens P; et al. Therapeutic efficacy of ^{213}Bi -labeled sdAbs in a preclinical model of ovarian cancer. *Mol. Pharmaceutics* 2020, 17, 3553–3566.
- (24). Pruszynski M; D'Huyvetter M; Bruchertseifer F; Morgenstern A; Lahoutte T Evaluation of an Anti-HER2 Nanobody Labeled with ^{225}Ac for Targeted α -Particle Therapy of Cancer. *Mol. Pharmaceutics* 2018, 15, 1457–1466.
- (25). Bateman TM Advantages and disadvantages of PET and SPECT in a busy clinical practice. *J. Nucl. Cardiol* 2012, 19, 3–11.
- (26). Queern SL; Aweda TA; Massicano AVF; Clanton NA; El Sayed R; Sader JA; Zyuzin A; Lapi SE Production of Zr-89 using sputtered yttrium coin targets. *Nucl. Med. Biol* 2017, 50, 11–16. [PubMed: 28376350]
- (27). Kraeber-Bodere F; Bailly C; Chérel M; Chatal J-F ImmunoPET to help stratify patients for targeted therapies and to improve drug development. *Eur. J. Nucl. Med. Mol. Imaging* 2016, 43, 2166–2168. [PubMed: 27539021]
- (28). Gebhart G; Lamberts L; Wimana Z; Garcia C; Emons P; Ameye L; Stroobants S; Huizing M; Aftimos P; Tol J; et al. Molecular imaging as a tool to investigate heterogeneity of advanced HER2-positive breast cancer and to predict patient outcome under trastuzumab emtansine (T-DM1): the ZEPHIR trial. *Ann. Oncol* 2016, 27, 619–624. [PubMed: 26598545]
- (29). Dijkers E; Oude Munnink T; Kosterink J; Brouwers A; Jager P; De Jong J; Van Dongen G; Schröder CP; Lub-de Hooge M; De Vries E Biodistribution of ^{89}Zr -trastuzumab and PET imaging of HER2-positive lesions in patients with metastatic breast cancer. *Clin. Pharmacol. Ther* 2010, 87, 586–592. [PubMed: 20357763]
- (30). Laforest R; Lapi SE; Oyama R; Bose R; Tabchy A; Marquez-Nostra BV; Burkemper J; Wright BD; Frye J; Frye S; et al. [^{89}Zr] Trastuzumab: evaluation of radiation dosimetry, safety, and optimal imaging parameters in women with HER2-positive breast cancer. *Mol. Imaging Biol* 2016, 18, 952–959. [PubMed: 27146421]
- (31). Dehdashti F; Wu N; Bose R; Naughton MJ; Ma CX; Marquez-Nostra BV; Diebold P; Mpoy C; Rogers BE; Lapi SE; et al. Evaluation of [^{89}Zr] trastuzumab-PET/CT in differentiating HER2-positive from HER2-negative breast cancer. *Breast Cancer Res. Treat* 2018, 169, 523–530. [PubMed: 29442264]
- (32). Ulaner GA; Hyman DM; Ross DS; Corben A; Chandarlapaty S; Goldfarb S; McArthur H; Erinjeri JP; Solomon SB; Kolb H; et al. Detection of HER2-positive metastases in patients with HER2-negative primary breast cancer using ^{89}Zr -trastuzumab PET/CT. *J. Nucl. Med* 2016, 57, 1523–1528. [PubMed: 27151988]
- (33). Bensch F; Brouwers AH; Lub-de Hooge MN; de Jong JR; van der Veegt B; Sleijfer S; de Vries EG; Schröder CP ^{89}Zr -trastuzumab PET supports clinical decision making in breast cancer patients, when HER2 status cannot be determined by standard work up. *Eur. J. Nucl. Med. Mol. Imaging* 2018, 45, 2300–2306. [PubMed: 30058029]
- (34). Ulaner GA; Lyashchenko SK; Riedl C; Ruan S; Zanzonico PB; Lake D; Jhaveri K; Zeglis B; Lewis JS; O'Donoghue JA First-in-human human epidermal growth factor receptor 2-targeted imaging using ^{89}Zr -Pertuzumab PET/CT: dosimetry and clinical application in patients with breast cancer. *J. Nucl. Med* 2018, 59, 900–906. [PubMed: 29146695]
- (35). Ulaner GA; Carrasquillo JA; Riedl CC; Yeh R; Hatzoglou V; Ross DS; Jhaveri K; Chandarlapaty S; Hyman DM; Zeglis BM; et al. Identification of HER2-positive metastases in patients with HER2-negative primary breast cancer by using HER2-targeted ^{89}Zr -pertuzumab PET/CT. *Radiology* 2020, 296, 370–378. [PubMed: 32515679]
- (36). Deri MA; Zeglis BM; Francesconi LC; Lewis JS PET imaging with ^{89}Zr : from radiochemistry to the clinic. *Nucl. Med. Biol* 2013, 40, 3–14. [PubMed: 22998840]
- (37). Meares CF; McCall MJ; Reardan DT; Goodwin DA; Diamanti CI; McTigue M Conjugation of antibodies with bifunctional chelating agents: isothiocyanate and bromoacetamide reagents, methods of analysis, and subsequent addition of metal ions. *Anal. Biochem* 1984, 142, 68–78. [PubMed: 6440451]

- (38). Vu T; Claret FX Trastuzumab: updated mechanisms of action and resistance in breast cancer. *Front. Oncol* 2012, 2, 62. [PubMed: 22720269]
- (39). Richard S; Selle F; Lotz J-P; Khalil A; Gligorov J; Soares DG Pertuzumab and trastuzumab: the rationale way to synergy. *An. Acad. Bras. Cienc* 2016, 88, 565–577. [PubMed: 27275646]
- (40). Maadi H; Soheilifar MH; Choi W-S; Moshtaghian A; Wang Z Trastuzumab mechanism of action; 20 years of research to unravel a dilemma. *Cancers* 2021, 13, 3540. [PubMed: 34298754]
- (41). Massicano AV; Bartels JL; Jeffers CD; Crenshaw BK; Houson H; Mueller C; Younger JW; Knapp P; McConathy JE; Lapi SE Production of [⁸⁹Zr] Oxinate4 and cell radiolabeling for human use. *J. Labelled Compd. Radiopharm* 2021, 64, 209–216.
- (42). D’huyvetter M; Vincke C; Xavier C; Aerts A; Impens N; Baatout S; De Raeve H; Muyldermans S; Caveliers V; Devoogdt N; et al. Targeted radionuclide therapy with A ¹⁷⁷Lu-labeled anti-HER2 nanobody. *Theranostics* 2014, 4, 708–720. [PubMed: 24883121]
- (43). Tchouate Gankam LO; Caveliers V; Devoogdt N; Vanhove C; Xavier C; Boerman O; Muyldermans S; Bossuyt A; Lahoutte T Localization, mechanism and reduction of renal retention of technetium-99m labeled epidermal growth factor receptor-specific nanobody in mice. *Contrast Media Mol. Imaging* 2011, 6, 85–92. [PubMed: 20936711]
- (44). Chatalic KL; Veldhoven-Zweistra J; Bolkestein M; Hoeben S; Koning GA; Boerman OC; de Jong M; van Weerden WM A novel ¹¹¹In-labeled anti-prostate-specific membrane antigen nanobody for targeted SPECT/CT imaging of prostate cancer. *J. Nucl. Med* 2015, 56, 1094–1099. [PubMed: 25977460]
- (45). Abou DS; Ku T; Smith-Jones PM In vivo biodistribution and accumulation of ⁸⁹Zr in mice. *Nucl. Med. Biol* 2011, 38, 675–681. [PubMed: 21718943]
- (46). Kumar SR; Quinn TP; Deutscher SL Evaluation of an ¹¹¹In-radiolabeled peptide as a targeting and imaging agent for ErbB-2 receptor-expressing breast carcinomas. *Clin. Cancer Res* 2007, 13, 6070–6079. [PubMed: 17947470]
- (47). Deutscher SL; Figueroa SD; Kumar SR ¹¹¹In-labeled KCCYSL peptide as an imaging probe for ErbB-2-expressing ovarian carcinomas. *J. Labelled Compd. Radiopharm* 2009, 52, 583–590.
- (48). Larimer BM; Thomas WD; Smith GP; Deutscher SL Affinity maturation of an ERBB2-targeted SPECT imaging peptide by in vivo phage display. *Mol. Imaging Biol* 2014, 16, 449–458. [PubMed: 24550054]
- (49). Fu R; Carroll L; Yahioğlu G; Aboagye EO; Miller PW Antibody fragment and affibody immunoPET imaging agents: radiolabelling strategies and applications. *ChemMedChem* 2018, 13, 2466–2478. [PubMed: 30246488]
- (50). Dekempeneer Y; Bäck T; Aneheim E; Jensen H; Puttemans J; Xavier C; Keyaerts M; Palm S; Albertsson P; Lahoutte T; et al. Labeling of anti-HER2 nanobodies with astatine-211: optimization and the effect of different coupling reagents on their in vivo behavior. *Mol. Pharmaceutics* 2019, 16, 3524–3533.
- (51). Pruszynski M; D’huyvetter M; Rodak M; Dekempeneer Y; Cedrowska E; Lahoutte T; Bruchertseifer F; Morgenstern A The therapeutic potential of anti-HER2 2Rs15d nanobody labeled with ²²⁵Ac-an in vitro and in vivo evaluation☆☆☆. *J. Med. Imaging. Radiat. Sci* 2019, 50, S73–S74.
- (52). Lacoueille F; Arlicot N; Faivre-Chauvet A Targeted alpha and beta radiotherapy: An overview of radiopharmaceutical and clinical aspects. *Med. Nucl* 2018, 42, 32–44.
- (53). Rodak M; Dekempeneer Y; Wojewódzka M; Caveliers V; Covens P; Miller BW; Sevenois MB; Bruchertseifer F; Morgenstern A; Lahoutte T; et al. Preclinical evaluation of ²²⁵Ac-labeled single-domain antibody for the treatment of HER2pos cancer. *Mol. Cancer Ther* 2022, 21, 1835–1845. [PubMed: 36129807]

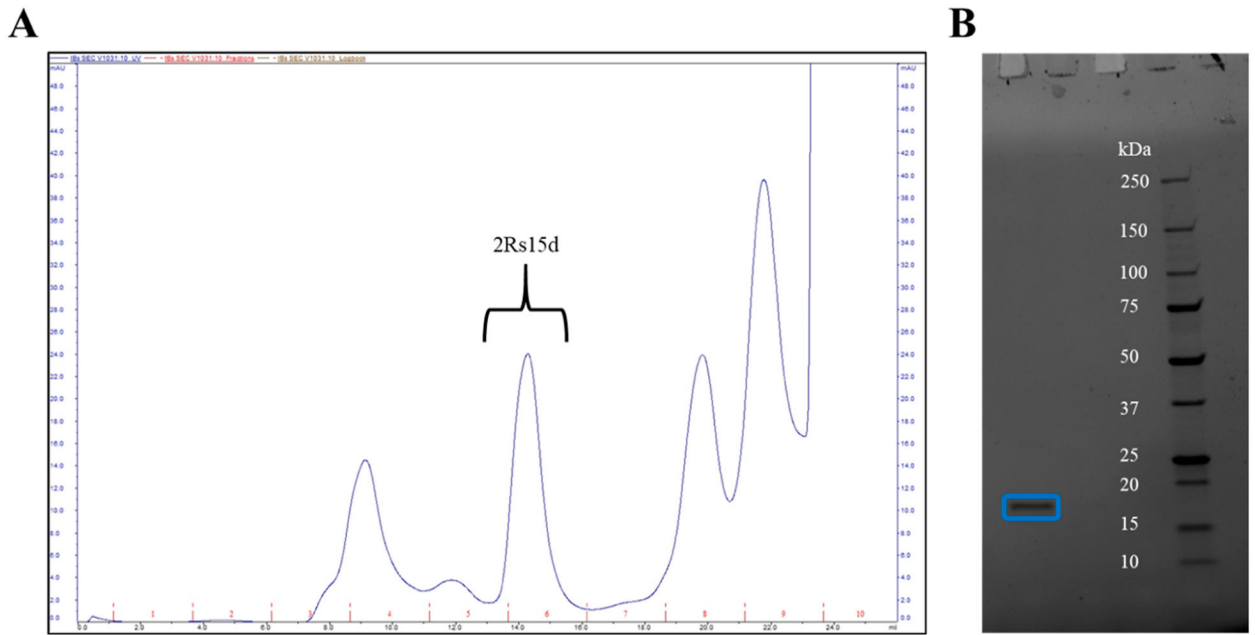


Figure 1. Purification of the 2Rs15d nanobody. (A) FPLC chromatogram showing the fraction collected of 2Rs15d with (B) the SDS-PAGE gel showing the molecular weight of ~17 kDa, confirming 2Rs15d production.

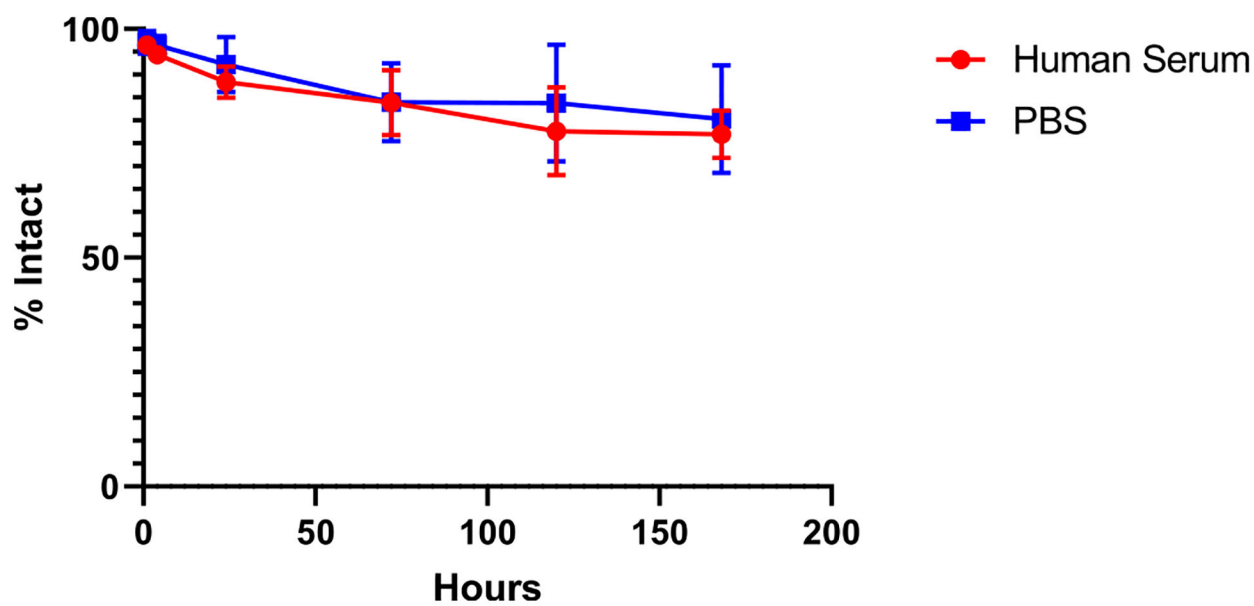


Figure 2. Stability of [^{89}Zr]Zr-DFO-2Rs15d up to 7 days in human serum and PBS. After 7 days, [^{89}Zr]Zr-DFO-2Rs15d was ~80% intact in both conditions. ($n = 6$ for each group).

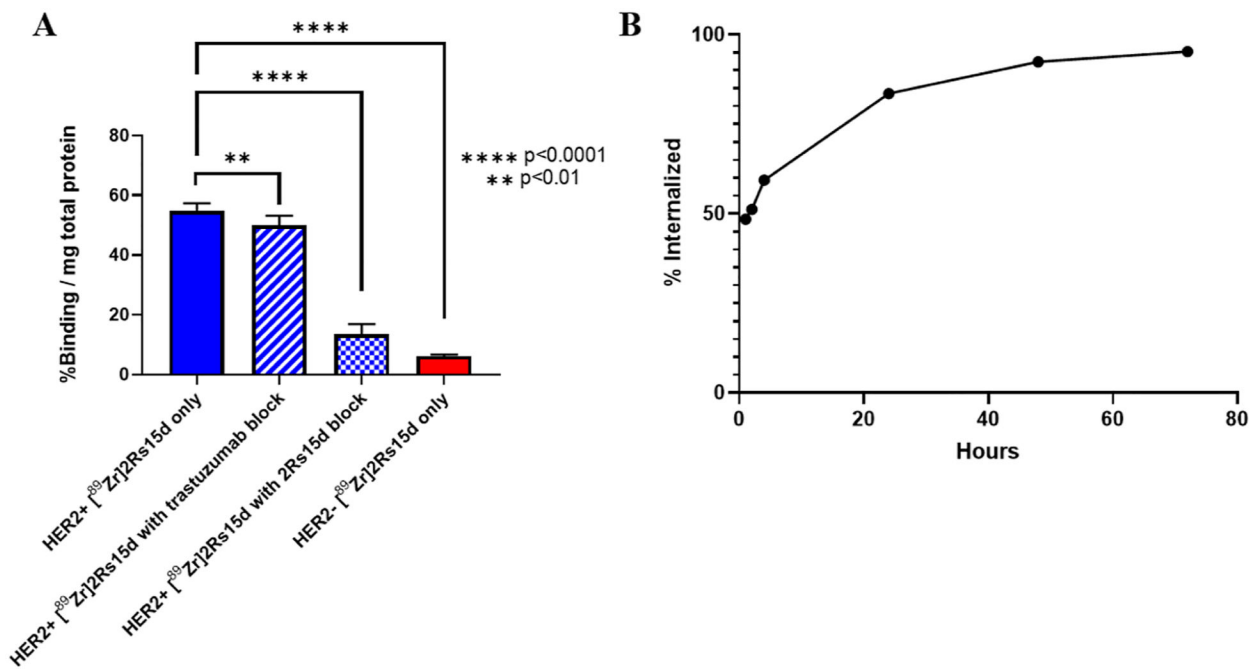


Figure 3. Cell binding studies evaluating [⁸⁹Zr]Zr-DFO-2Rs15d. (A) Cell binding and specificity studies show [⁸⁹Zr]Zr-DFO-2Rs15d has specific binding to HER2 while binding to a different epitope than trastuzumab. (*n* = 8 for each group) (B) Internalization studies showed a steady increase of cell-associated [⁸⁹Zr]Zr-DFO-2Rs15d internalized over 72 h. (*n* = 6 for each group) ***p* < 0.01 and *****p* < 0.0001.

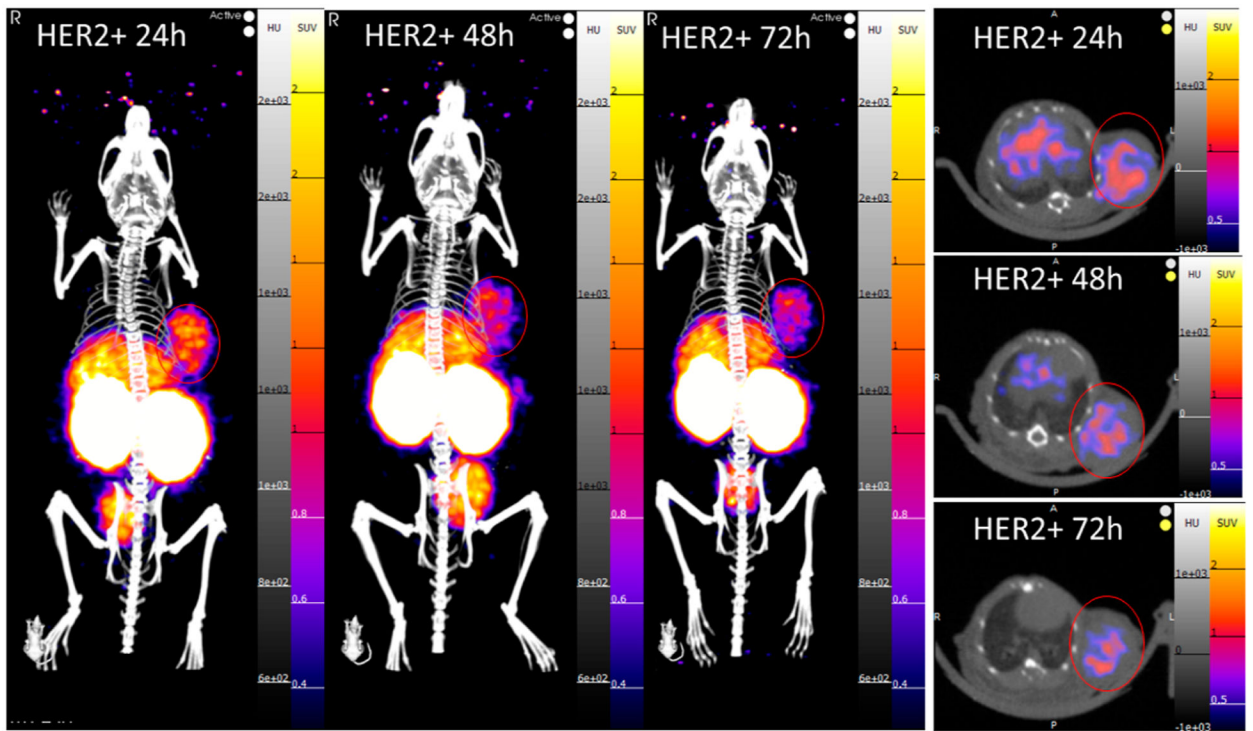


Figure 4. PET/CT images at 24, 48, and 72 h postinjection of a HER2-positive tumor-bearing mouse (SUVmean scale 0.3–2). The tumor can be clearly visualized on the left shoulder of the mouse at all time points in both the maximum intensity projection (MIP) and transverse slice images.

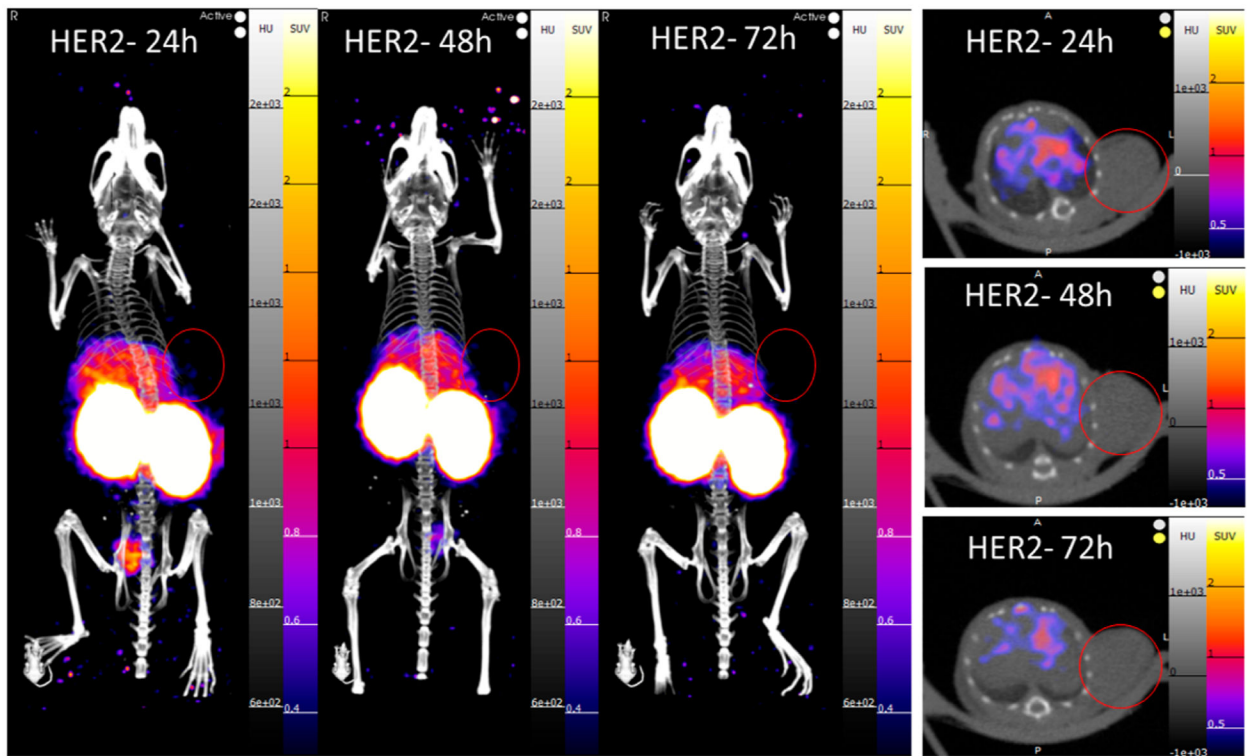


Figure 5. PET/CT images at 24, 48, and 72 h postinjection of a HER2-negative tumor-bearing mouse (SUVmean scale 0.3–2). No PET signal could be visualized in the tumor at the selected window to compare with the HER2-positive mice. The tumor is located on the left shoulder in the same area as the HER2-positive tumor-bearing mice.

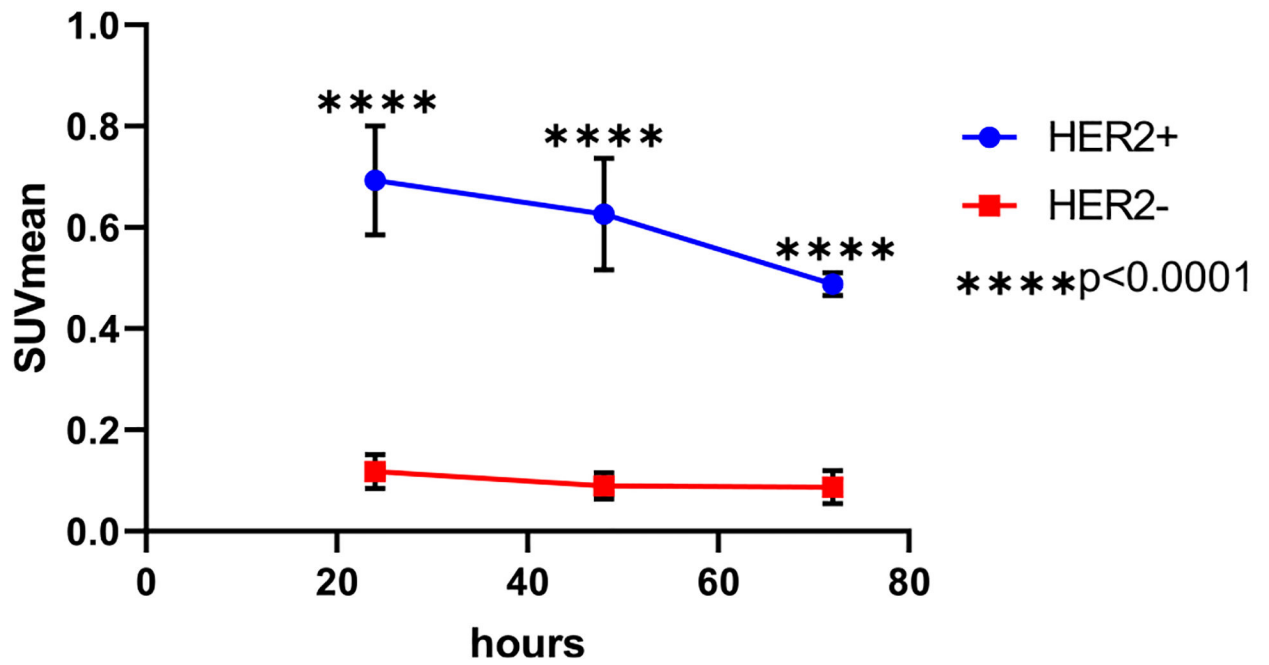


Figure 6. HER2-positive tumors had a higher SUVmean than HER2-negative tumors at 24, 48, and 72 h postinjection of [^{89}Zr]Zr-DFO-2Rs15d. Analysis was completed using a student's *t*-test. **** $p < 0.0001$.

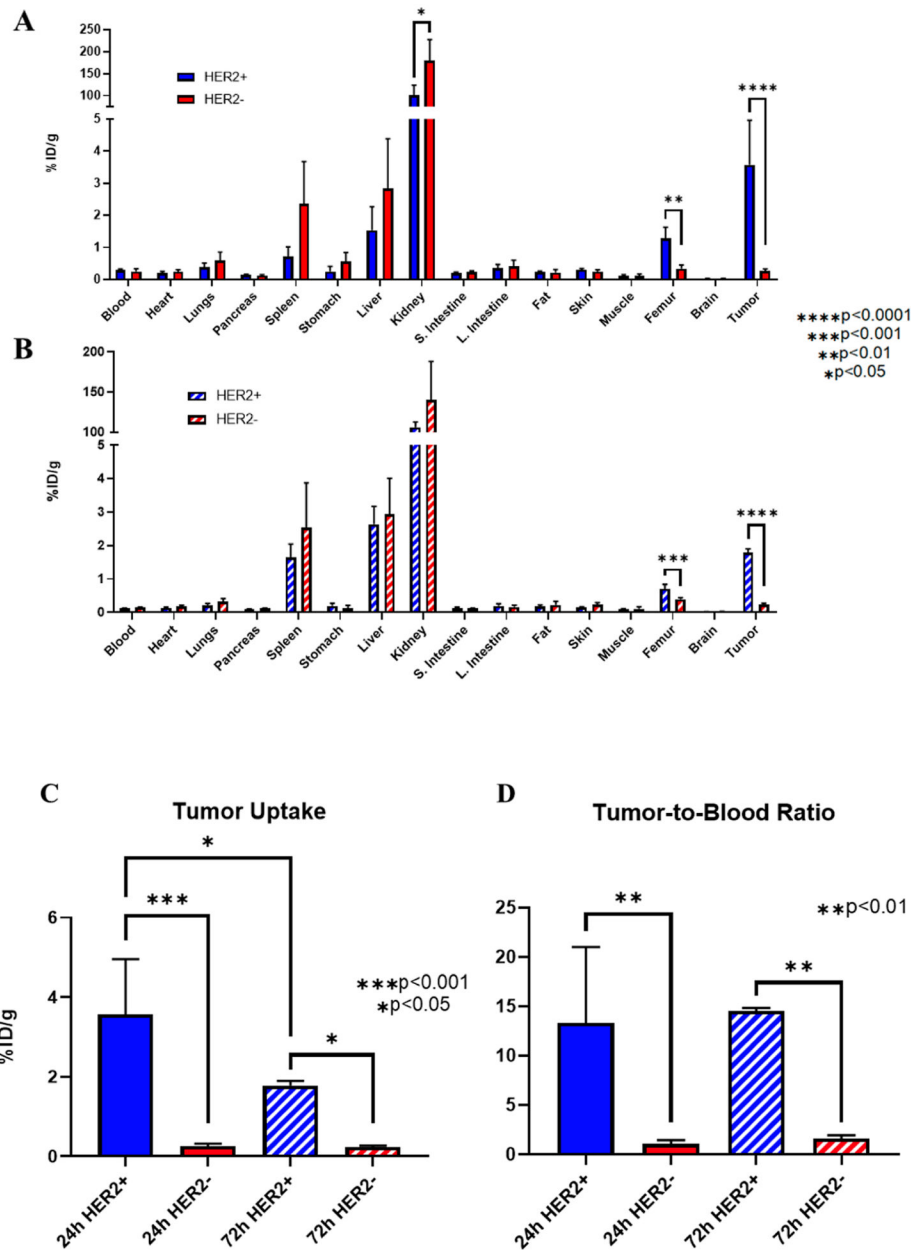


Figure 7. Biodistribution of [⁸⁹Zr]Zr-DFO-2Rs15d in HER2-positive and HER2-negative tumor-bearing mice. Full body biodistribution at (A) 24 h and (B) 72 h shows high kidney radioactivity levels with modest liver, spleen, and femur uptake. (C) HER2-positive tumors had significantly higher tumor uptake and (D) tumor-to-blood ratios of [⁸⁹Zr]Zr-DFO-2Rs15d compared to HER2-negative tumors at both time points. (*n* = 4 for all groups). **p* < 0.05, ***p* < 0.01, ****p* < 0.001, and *****p* < 0.0001.